

ORIGINAL ARTICLE

Role of 3-Dimensional Architecture of Scar and Surviving Tissue in Ventricular Tachycardia

Insights From High-Resolution Ex Vivo Porcine Models

BACKGROUND: An improved knowledge of the spatial organization of infarct structure and its contribution to ventricular tachycardia (VT) is important for designing optimal treatments. This study explores the relationship between the 3-dimensional structure of the healed infarct and the VT reentrant pathways in high-resolution models of infarcted porcine hearts.

METHODS: Structurally detailed models of infarcted ventricles were reconstructed from ex vivo late gadolinium enhancement and diffusion tensor magnetic resonance imaging data of 8 chronically infarcted porcine hearts at submillimeter resolution ($0.25 \times 0.25 \times 0.5 \text{ mm}^3$). To characterize the 3-dimensional structure of surviving tissue in the zone of infarct, a novel scar-mapped thickness metric was introduced. Further, using the ventricular models, electrophysiological simulations were conducted to determine and analyze the 3-dimensional VT pathways that were established in each of the complex infarct morphologies.

RESULTS: The scar-mapped thickness metric revealed the heterogeneous organization of infarct and enabled us to systematically characterize the distribution of surviving tissue thickness in 8 hearts. Simulation results demonstrated the involvement of a subendocardial tissue layer of varying thickness in the majority of VT pathways. Importantly, they revealed that VT pathways are most frequently established within thin surviving tissue structures of thickness $\leq 2.2 \text{ mm}$ (90th percentile) surrounding the scar.

CONCLUSIONS: The combination of high-resolution imaging data and ventricular simulations revealed the 3-dimensional distribution of surviving tissue surrounding the scar and demonstrated its involvement in VT pathways. The new knowledge obtained in this study contributes toward a better understanding of infarct-related VT.

VISUAL OVERVIEW: An online [visual overview](#) is available for this article.

Farhad Pashakhanloo, PhD
Daniel A. Herzka, PhD
Henry Halperin, MD
Elliot R. McVeigh, PhD
Natalia A. Trayanova, PhD

Key Words: arrhythmias, cardiac
■ computer simulation ■ magnetic
resonance imaging ■ myocardial
infarction ■ tachycardia, ventricular

© 2018 American Heart Association, Inc.

<http://circep.ahajournals.org>



WHAT IS KNOWN?

- Surviving myocardium in the zone of infarct plays an important role in infarct-related ventricular tachycardias (VTs) by providing conduction pathways for reentry.
- Knowledge of the spatial organization of scar and surviving tissue and its contribution to infarct-related VT is paramount to designing optimal treatments for VT.

WHAT THE STUDY ADDS?

- Using ex vivo high-resolution (submillimeter) late gadolinium enhancement magnetic resonance imaging scans and a new scar-mapped local thickness metric, the study revealed the complex distribution of surviving tissue within the infarct in porcine hearts and provided systematic quantification of the thickness of surviving tissue in these hearts in a nondestructive way.
- Simulations with the high-resolution models reconstructed from the magnetic resonance imaging scans demonstrated that 3-dimensional VT pathways were established through surviving tissues (whether channels or layers) with varying thickness, with the involvement of subendocardial tissue in the majority of the VTs. The VT pathways were preferentially localized within surviving tissue structures with smaller thickness (90th percentile of <2.2 mm).

Ventricular tachycardia (VT) is a life-threatening rapid heart rhythm disorder that frequently occurs in the presence of myocardial infarction (MI).¹ Structural and electrophysiological remodeling associated with the infarct causes conduction irregularities that can lead to the formation of reentrant circuits in the heart.^{2,3} Reentry has been identified as a major mechanism underlying VT associated with healed or healing MI in the human.⁴ The formation of reentrant circuits associated with MI is a complex phenomenon that depends on factors ranging from the cellular scale to the whole heart.³ Of particular importance is the spatial distribution of the scar and the surviving tissue in the zone of infarct because the mixture of the 2 tissues can form complex tortuous pathways for electrical activation.^{5–10} Accurate characterization of the tissue architecture within the zone of infarct is, therefore, essential for the complete understanding of the mechanisms of infarct-related reentrant arrhythmias.

The current gold standard for noninvasive imaging of MI in patients is clinical late gadolinium enhancement (LGE) magnetic resonance imaging (MRI).¹¹ MI signal intensity information from LGE-MRI has been correlated with endocardial voltage maps.^{12,13} It has also been used to identify conducting channels^{14,15} and critical isthmus sites of VT in the infarct.^{16–18} More-

over, MI signal intensity characteristics in LGE-MRI have been demonstrated to be a strong predictor for global susceptibility to arrhythmia and postinfarction mortality.^{19–21} Despite the utility of clinical LGE-MRI in identifying potential substrates for VT and assessing risk for arrhythmias, its limited spatial resolution in human imaging hinders the accurate characterization of the underlying 3-dimensional (3D) structure and conductive pathways in the zone of infarct involved in VT.

Ex vivo imaging of large animal and human hearts allows data acquisition at high spatial resolution and image quality, which is otherwise impossible to achieve in a beating heart. Ex vivo MRI data have been used in many studies to characterize the structure of the human and large animal hearts under normal²² and disease^{23,24} conditions. It has also enabled construction of individualized computational models of such hearts to explore arrhythmia mechanisms.^{25–28} A comprehensive investigation of the role of infarct structure on arrhythmias at the whole heart level requires, however, computational models that capture the complex geometry of the infarct; therefore, the images must resolve the intricate features of the scar at a resolution higher than achieved previously, such as submillimeter resolution. Such models could provide new insights on the VT mechanisms and lead to an improved interpretation of clinical recordings of electrical activity in the zone of infarct.

The 2 primary goals of the current study are: (1) to use high-resolution (submillimeter) whole-heart ex vivo MRI data to characterize the 3D structure of the surviving myocardium within the zone of infarct and (2) to use whole ventricular modeling to investigate the VT pathways emerging from the complex architecture of 3D scar and surviving tissue surrounding it. An improved knowledge of the spatial organization of the infarct in high resolution and its contribution to arrhythmia is important for designing optimal treatments for VT.

METHODS

The data, analytic methods, and study materials will be made available to other researchers for purposes of reproducing the results or replicating the procedure.

LGE and Diffusion Tensor MRI Data Acquisition

The ventricular data used here was acquired in a previous study using high-resolution ex vivo LGE and diffusion tensor (DT) MRI techniques in 8 chronically infarcted porcine hearts with anteroseptal infarction (MI age, 6.9±2.9 months),²⁴ in accordance with the Johns Hopkins University Institutional Animal Care and Use Committee. LGE imaging provided detailed information about ventricular and infarct geometries. Images were obtained using a T1-weighted gradient echo sequence with the following scan parameters: acquired resolution, 0.25×0.25×0.50 mm³; reconstructed voxel size, 0.25×0.25×0.25 mm³; echo time,

2.3 ms; repetition time, 12 ms; flip angle, 15°; and scan duration, 1 hour (see the [Data Supplement](#) for a description of specimen preparation before ex vivo imaging). The DT-MRI acquisition in the same hearts provided data on the subject-specific fiber orientation; it was performed using a customized 3D spin echo sequence.²² The acquired and reconstructed voxel dimensions for the diffusion images were 0.6×0.6×1.2 and 0.4 mm³, respectively, and the total scan duration was ≈42 hours per heart. The primary eigenvectors of the DTs were calculated to determine the local orientation of the myofibers. Detailed methodology, including data acquisition and sample preparation, can be found in previous publications.^{22,24}

Ventricular Model Construction

We used the acquired ex vivo data, as described above, to construct, for the first time, detailed models of the intact large animal ventricles with infarction, with image-based fiber orientation and detailed scar geometry obtained at a voxel size of 0.03125 mm³ (≈400× smaller than that of clinical MRI). First, the left and right ventricles were segmented using an intensity-based thresholding of the LGE images to suppress the dark background. Then, an Otsu thresholding ($n=2$ regions) followed by a level-set segmentation algorithm was applied to separate heart tissue into regions of (enhanced) scar and (nonenhanced) myocardium (Figure 1A, left). The epicardial fat tissue and other image artifacts were removed from the segmentations using manual contouring and intensity-based thresholding. Further, a 3D finite-element mesh with tetrahedral elements was constructed for each heart from the segmented myocardial images using ScanIP software (Simpleware, Ltd, United Kingdom). This process yielded volumetric meshes with locally adaptive spatial resolution to accurately preserve the fine details of the scar boundary (Figure 1A, right). A typical generated mesh had ≈4 million nodes and ≈20 million tetrahedral elements with an average edge length of ≈350 μm. Fiber orientation was mapped onto each ventricular mesh from the corresponding DT-MRI data set.²⁴

Cardiac Electrophysiology Simulation and In-Silico VT Induction

The constructed models were used in whole-heart arrhythmia simulations to study, in high resolution, the reentrant pathways and their relation to the detailed infarct structure. Electrical wave propagation was modeled by the monodomain formulation, and the simulations were performed using the software package CARP (CardioSolv, LLC) on a parallel computing platform; numeric details of the finite-element simulations have been described in previous publications.^{29–31} Myocyte membrane kinetics were represented by the Luo-Rudy dynamic model³²—a generic mammalian membrane model used in numerous studies of arrhythmia. Given the medium-to-low complexity of the Luo-Rudy dynamic model, it is a reasonable trade-off in large-scale models, such as the whole porcine heart. Scar tissue was modeled as an electrical insulator by removing the scar internal nodes from the mesh in the simulations. Additional details on the infarct modeling methodology

are presented in the [Data Supplement](#). Monomorphic VTs were induced in all the hearts using a clinical S1-S2-S3 programmed electrical stimulation protocol³¹ that was applied from 27 pacing sites selected on the basis of a modified American Heart Association segment designation in each heart (Figure 1B; see also Figure I in the [Data Supplement](#)). The large number of pacing locations (relative to a clinical protocol) ensures that we can capture a wide range of possible VT morphologies that could arise from a given infarct morphology, therefore, fully exploring the relationship between VT pathways and infarct structure. Finally, pseudo-ECG waveforms were calculated for each VT episode from the difference of the extracellular potentials of 2 virtual electrodes each positioned 5 cm away from the left and the right base of the heart.

Quantification of the Thickness of Surviving Tissue Surrounding the Scar

In all hearts, the infarcted sections of the wall were composed of a spatially complex interdigitation of (enhanced) scar and (nonenhanced) surviving tissue surrounding the scar. To characterize the structure of the surviving tissue surrounding the scar, we defined a novel scar-mapped local thickness (SMLT) metric. This metric was calculated for each point on the 3D surface of the scar as described below.

At each point on the 3D scar surface, a line was extended in the direction normal to the surface (Figure 1C, middle) until it intersected with another surface, either that of scar, or epicardium, or endocardium. The thickness metric was defined as the minimum of l and $2d_{\max}$, where l is the length of the normal line (shown in red) and d_{\max} is the largest distance to the closest surface calculated at each tissue point along the red normal line. Finding d_{\max} was needed to account for cases where the normal line is oblique to the surface it intersects because l would overestimate the thickness (see also Figure II in the [Data Supplement](#)). Next, the 3D scar surface was color coded at each point with the local value of the thickness metric (Figure 1C, right). As illustrated in the figure, the thickness of the surviving myocardium increases toward the edges of the scar (red color in the map). Such maps provide an efficient and systematic way to characterize the local thickness of the myocardium surrounding the patches of scar that would otherwise be difficult to detect and visualize because of the complex architecture. Additional detail on the calculation of the SMLT metric is presented in the [Data Supplement](#).

Analysis of Reentry Pathways

The sustained VTs (defined as lasting for at least 2 seconds after the last pacing stimulus) were analyzed to obtain information on VT morphology and cycle length (CL). To identify the 3D morphology of each VT pathway, we connected seed points along the fastest part of the 3D route of each VT as it completes 1 cycle, thus reducing the reentry, for analysis, to a simplified continuous string loop within the 3D ventricle. Within the confines of each loop, there is only unexcited tissue, either scar, or excitable tissue in which propagation fails. The reentry path length is defined as the length of this string loop. Next, to characterize the local thickness of the tissue that contributes to reentry,

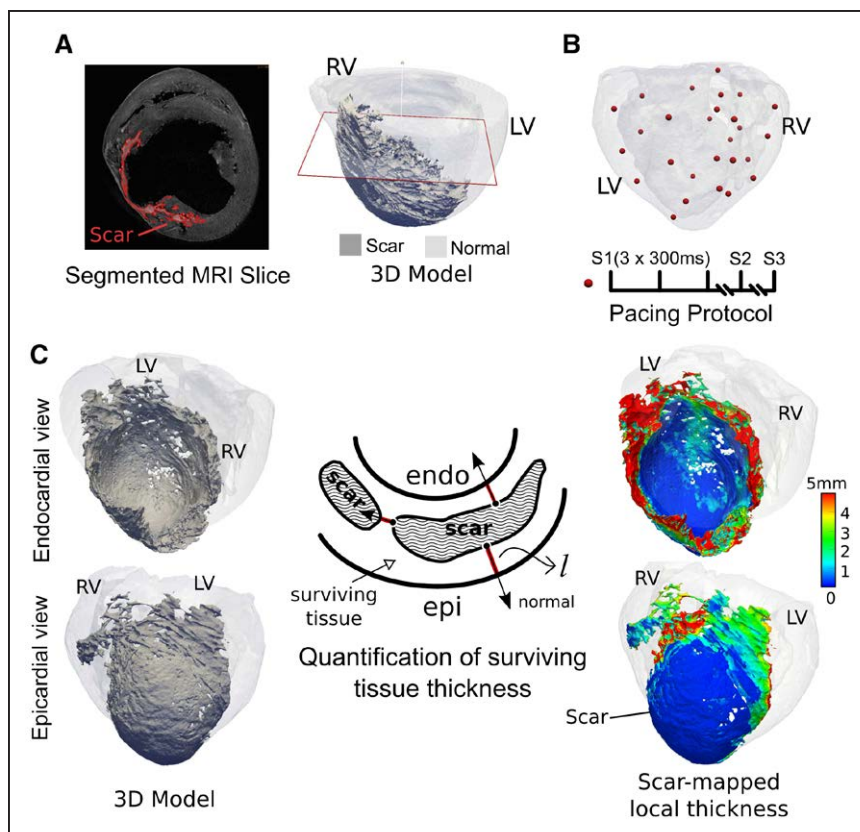


Figure 1. Workflow of the study, including imaging, model construction, ventricular tachycardia simulation protocol, and the calculation of scar-mapped local thickness (SMLT) metric.

A, Left, A short-axis slice of late gadolinium enhancement-magnetic resonance imaging (MRI) acquired at the voxel size of $0.25 \times 0.25 \times 0.5$ mm³. The segmented scar is highlighted in red. **Right**, Three-dimensional (3D) reconstructed model of the same heart with the scar highlighted in dark gray and myocardium in transparent gray. The red plane shows the location of the short-axis MRI slice that is displayed in the (left). **B**, Pacing protocol. **Top**, 3D distribution of pacing locations. **Bottom**, stimulus train (S1, S2, and S3). **C**, Calculation of surviving tissue thickness surrounding the scar using SMLT metric. The schematic in the middle illustrates a cross section of the wall composed of scar and surviving tissue. The red lines are extended from the scar surface in the direction of the normal vector to the scar surface. The calculated local thickness of the surviving tissue is mapped onto the scar surface and displayed in endocardial and epicardial views on the (right; see Methods for detailed description). endo indicates endocardium; epi, epicardium; LV, left ventricle, and RV, right ventricle.

each point along the pathway was assigned the SMLT metric value from the closest scar surface point. To do so, the points along each 3D pathway were first interpolated to obtain a consistent 100- μ m distance between them. This enabled us to obtain a distribution of the surviving tissue thickness values along the reentry pathway.

RESULTS

Characterization of Surviving Tissue Surrounding the Scar

All the hearts had anteroseptal infarcts with significant wall thinning at each region of infarct. One of the hearts exhibited an additional enhanced area in the lateral wall because of a second infarction (heart 8). The extent of the infarct across the wall was variable, but the scar was preferentially localized in the subendocardial half of the wall.²⁴ Regions of nonenhanced (viable) tissue interdigitated with scar patches were frequently observed, either adjacent to the scar subendocardially or subepicardially, or located intramurally traversing the scar. Three representative examples of viable tissue distribution are presented in Figure 2, as delineated in short-axis slices of high-resolution LGE-MRI. In Figure 2A, there is a thin layer of subendocardial surviving tissue of varying thickness. In Figure 2B, surviving tissue at the midwall provides a conductive pathway through the distributed scar. In Figure 2C, a region of viable myocardium is observed adjacent to the scar at

the subepicardium, with a gradual decrease in its thickness from right to left.

Figure 3A presents the SMLT metric in all 8 hearts. These maps demonstrate the complex 3D anatomy of the scar with the color coding revealing the spatial organization and the extent of surviving tissue surrounding scar patches. The lighter blue and green areas of the map indicate the presence of surviving tissue with thickness range of 0.5 to 3.0 mm overlaying the scar, whereas the darker blue regions represent thinner tissues (<0.5 mm) or indicate the absence of viable tissue on the endocardial or epicardial surfaces of the scar (ie, if the scar extends all the way to the surface). As illustrated by these maps, the surviving tissue surrounding the scar has a complex spatial organization with variable thickness.

Further, the SMLT metric values were aggregated over the scar surface of each heart; Figure 3B presents the normalized and cumulative histograms in the individual hearts, as well as pooled data from all the hearts. These histograms illustrate the frequency of occurrence of surviving tissue with different thickness values at the zone of infarct. The median and (25th–75th) percentile values of the pooled thickness distribution were 1.1 mm and 0.6 to 2.1 mm, respectively.

VTs Induced in Ventricular Models

In all the heart models, pacing-induced propagation through the infarct zones was heterogeneous, as illus-

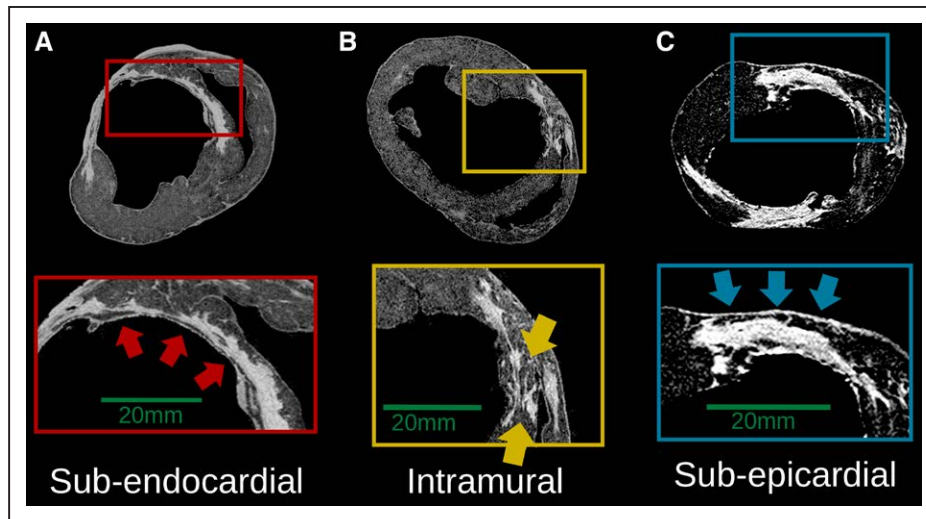


Figure 2. Examples of the distribution of viable tissue in the zone of infarct, as visible from short-axis slices of high-resolution late gadolinium enhancement-magnetic resonance imaging in 3 infarcted hearts (5, 7, and 8).

A, Thin subendocardial layer of surviving tissue (red arrows); **B)** intramural viable tissue (yellow arrows); **C)** subepicardial layer of surviving myocardium (blue arrows).

trated by the complex isochrones in 2 of the heart models in Figure III in the [Data Supplement](#). From a total of 216 attempts to induce reentry following the pacing protocol, 72 attempts led to sustained monomorphic VTs. Among those, 23 unique VT morphologies were identified (equivalent to 2.9 ± 1.8 morphologies per heart). The average VT CL was 190 ± 59 ms. This value is consistent with that of experimentally recorded VTs in porcine hearts³³ (average values match within $\pm 5\%$). Eleven of the 23 VT morphologies were induced from >1 pacing location. Detailed characteristics of the VTs are provided in Table I in the [Data Supplement](#).

Figures 4 through 6 present 3 examples of infarct-related VTs. Figure 4 illustrates a subendocardial VT in heart 6 (CL, 145 ms; Movie I in the [Data Supplement](#)). The infarct spans the septum and the anterior wall (Figure 4A and 4B). The VT is depicted at different time points using transmembrane voltage maps (Figure 4C through 4E); the pseudo-ECG shows sustained VT after pacing (Figure 4F). As the voltage maps demonstrate, the reentrant circuit is primarily located on the endocardial side of the scar. The SMLT map in Figure 4B reveals the heterogeneity in the thickness of the surviving subendocardial tissue that creates tortuous pathways for the activation during reentry.

Figure 5 presents a subepicardial reentry in heart 5 (CL, 230 ms; Movie II in the [Data Supplement](#)). In this case, the reentry encompasses propagation through a tube-like structure of viable tissue that runs inside the infarct subepicardially. The channel has an irregular zig-zag shape with total length of ≈ 30 mm (Figure 5C). The total activation time inside the channel is ≈ 120 ms. This channel contributed to 1 sustained VT (Figure 5E) and 8 unsustained reentries induced from multiple pacing sites.

In addition to the VT circuits in which the reentry pathway is contained within the tissue on one side of the scar (either subepicardially or subendocardially), as demonstrated in the previous figures, some VTs involved propagation that traversed the scar transmurally and made breakthroughs at the epicardial or endocardial surface. An example of such reentry is presented in Figure 6A (CL, 240 ms; Movie III in the [Data Supplement](#)). The activation wave front travels transmurally through a region of surviving tissue in the infarct zone (green in Figure 6B) and makes a breakthrough on the epicardium. This reentry morphology was inducible from 11 pacing locations in this heart. Another example of a transmural VT with breakthroughs both on endocardium and epicardium is presented as Figure IV in the [Data Supplement](#).

As presented in Table I in the [Data Supplement](#), the majority of the VT pathways were completely or partially subendocardial (52% and 78%, respectively), whereas 26% of the simulated VTs traversed the scar transmurally with breakthroughs at the epicardium and the endocardium. Finally, 22% of the pathways were located entirely at the epicardial side of the scar.

Characterization of VT Pathways and the Contributing Surviving Tissue

The average path length for the 23 VT morphologies was 53 ± 14 mm. Figure 7A and 7C present all the VT pathway loops in hearts 5 and 6. For each heart, the corresponding distribution of the SMLT metric is presented in Figure 7B and 7D, respectively. In these plots, the blue histograms represent the frequencies of occurrence of a given thickness value over the entire 3D scar surface in each heart, whereas the red histo-

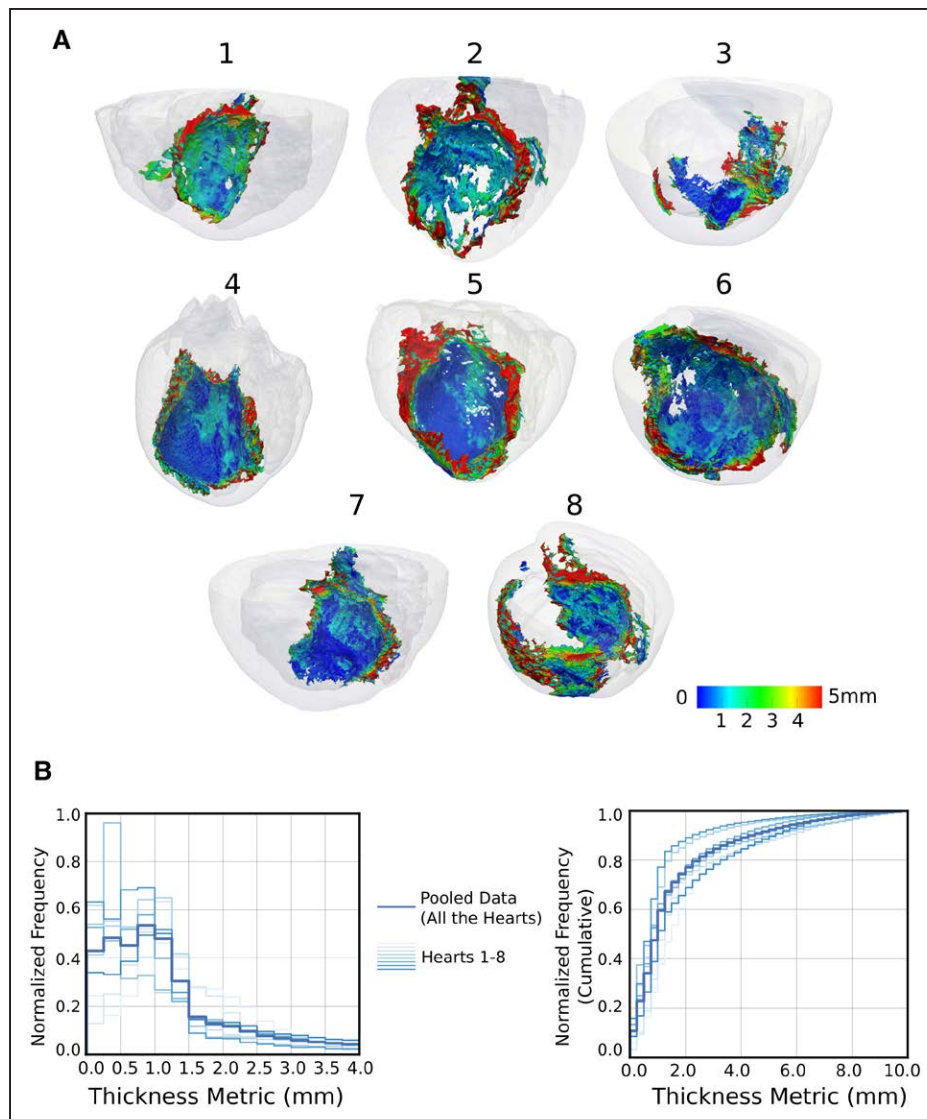


Figure 3. Visualization and characterization of surviving tissue surrounding the scar.

A, 3-dimensional geometries of 8 infarcted hearts with the scar surface color coded with scar-mapped local thickness (SMLT) metric. The hearts are viewed from the posterolateral side such that the endocardial aspect of the infarct is visible. **B**, Histograms of the occurrence of surviving tissue at different SMLT metric values, calculated in all the 8 hearts ([left] normalized and [right] cumulative histograms).

grams represent these frequencies for the subset of points belonging to VT pathways.

Further, in Figure 7E, aggregated normalized (left) and cumulative (right) histograms of SMLT are presented for all the 23 VTs in the 8 hearts in the study (red). Similarly, in the same figure, SMLT histograms for the entire 3D scar surface in all hearts are plotted in blue. Despite similarities in the shape of the distributions, the red histogram is preferentially localized toward smaller tissue thickness. As the figure demonstrates, a major portion of the VT pathways (90%) is through viable tissue of thickness <2.2 mm. The median and the (25th–75th) percentile values of the distribution were 0.94 mm and 0.6 to 1.3 mm, respectively, with $\approx 7\%$ of the pathways points located in regions with thickness ≤ 0.25 mm.

DISCUSSION

The goal of this study was to explore the relationship between the complex 3D structure of the healed infarct and the 3D VT pathways in high-resolution models of infarcted porcine hearts. To do so, structurally detailed models of infarcted ventricles were reconstructed from previously acquired²⁴ ex vivo LGE and DT-MRI data of 8 chronically infarcted porcine hearts at a voxel size >400-fold smaller than clinical LGE-MRI. A scar-mapped metric, SMLT, was defined that provided a novel means to quantify the structure of the surviving tissue surrounding the scar. This method revealed the heterogeneous spatial organization of surviving tissue within the infarct and enabled us to systematically characterize the thickness distribution of surviving tissue in the infarct vol-

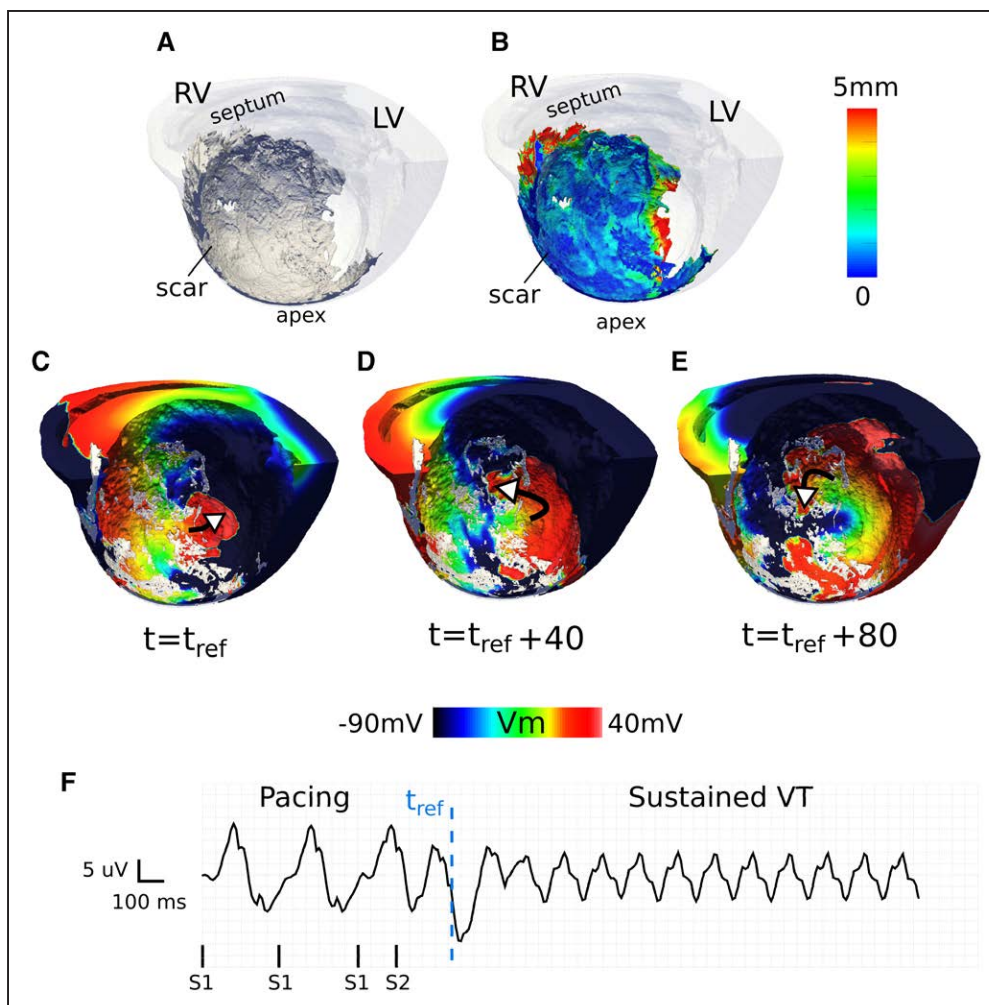


Figure 4. A representative ventricular tachycardia (VT) sustained primarily within a heterogeneous layer of subendocardial viable tissue (cycle length, 145 ms) shown in an endocardial view of the septum in heart 6.

A, Three-dimensional (3D) geometry (scar, dark gray; myocardium, transparent white). **B**, 3D geometry with the scar color coded with the scar-mapped local thickness metric. **C–E**, Transmembrane voltage maps demonstrating time snapshots of tortuous wave propagation in 1 cycle of reentry. White arrows show wave direction. The reentry is primarily located in the subendocardial layer of tissue. **F**, Pseudo-ECG. t_{ref} : reference time. LV indicates left ventricle, and RV, right ventricle.

umes of 8 hearts. Constructing high-resolution ventricular models from the imaging data, we were able to simulate and analyze the VT pathways that are established for each of the complex infarct morphologies. The results demonstrated that the VT pathways are established through surviving tissues (whether channels or layers) with varying thickness. It also showed the involvement of subendocardial tissue in 78% of VT pathways. Importantly, the analysis revealed that VT pathways are preferentially established within surviving tissue structures of thickness of 0.25 to 1.75 mm, with the majority of the pathway portions traversing thin tissues of ≤ 2.2 mm (90th percentile) surrounding the scar.

Identification and Characterization of Viable Tissue Surrounding the Scar

A major contribution of this study is the characterization of the 3D architecture of viable myocardium surrounding the scar in intact hearts. The presence of sur-

ving myocardial fibers in the healed infarct has been shown previously by means of sectioning the heart.^{5,34} In agreement with these studies, we found complex regions of viable tissue embedded in the infarct; these regions surrounded the scar at the subendocardium or subepicardium or penetrated the scar intramurally. Efficient visualization and quantification of the thickness of such surviving regions is challenging because of their irregular 3D shape. The novel SMLT maps introduced here provide a systematic way to identify and characterize the dimension of these structures. Using the thickness maps, we identified diverse morphologies of viable tissue surrounding the scar, including tube-like channels within subepicardial layer, small regions of viable tissue inside the scar connecting the endocardium and epicardium, and sheets of surviving myocardium at the subepicardium or subendocardium with varying thickness throughout the infarct. Aggregation of the SMLT values over the surface of all scar patches in each heart and in all hearts combined allowed us to construct, for

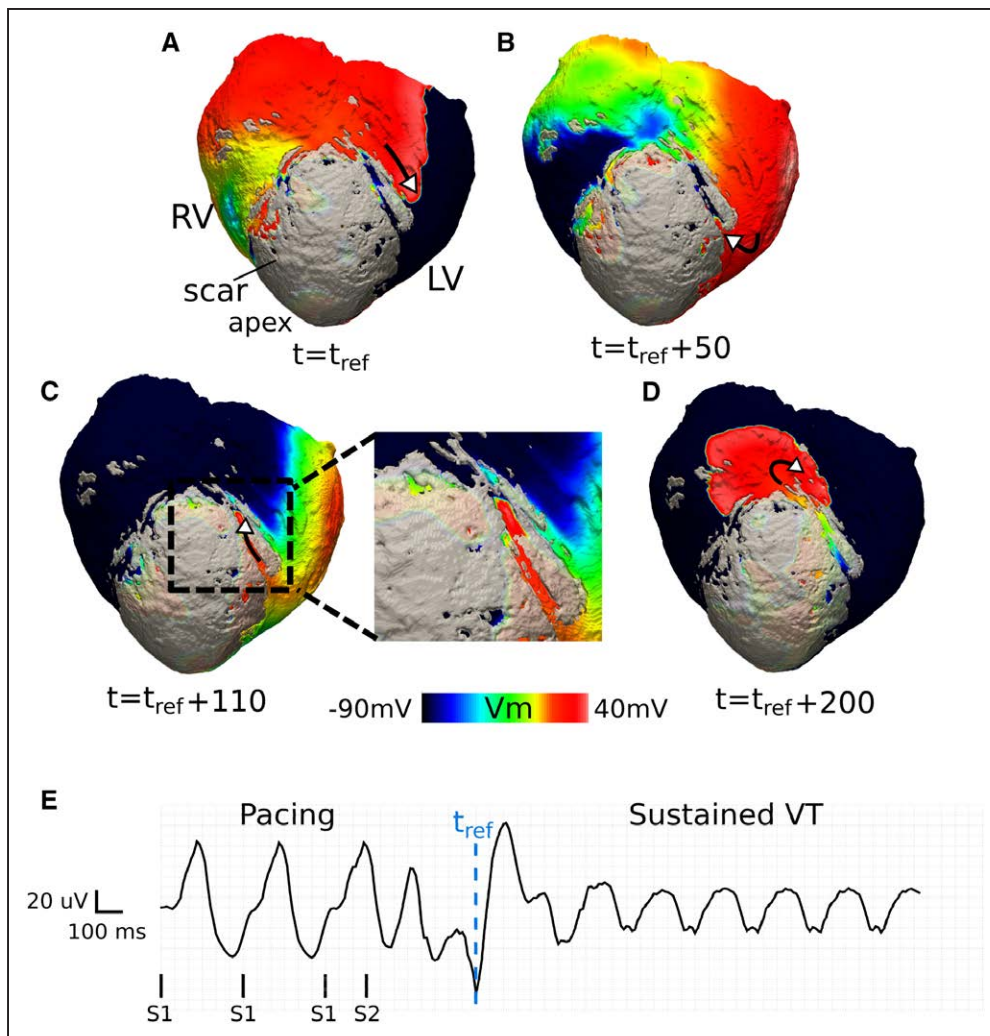


Figure 5. Reentry involving a subepicardial channel of viable tissue in heart 5 (cycle length, 230 ms).

A–D. Transmembrane voltage maps showing 1 cycle of reentry. The wave traverses the channel in **B** and **C**; its exit from the channel is followed by a centrifugal activation of the tissue outside the scar in **D**. The length of the epicardial channel is ≈ 30 mm, and the ventricular tachycardia (VT) path length is 74 mm. A border layer around the scar has been rendered semitransparent to visualize channel position. **E.** Pseudo-ECG. t_{ref} : reference time. LV indicates left ventricle, and RV, right ventricle.

the first time, distribution plots that revealed the frequency at which each surviving tissue thickness value occurs in these infarcts.

Link Between Viable Tissue Structure Surrounding the Scar and VT Pathways

Previous experimental studies have suggested that the viable myocardium surrounding the scar plays a role in ventricular arrhythmias.^{33,34} However, in those studies, VTs were mapped at low resolution, and mapping was limited to the endocardial or epicardial surfaces; thus, the 3D patterns of the VTs within the 3D infarct structure could not be explored. In this study, using image-based simulations, we examined and visualized VT morphologies in 3 dimensions and correlated the VT pathways to the 3D surviving tissue structure in high resolution. The aggregated histograms for the thickness of the surviving tissue constructed using the SMLT metric, one represent-

ing the total amount of surviving tissue surrounding the scar (Figure 7E, blue) and the other representing only surviving tissue part of the VT pathways (Figure 7E, red), show important differences. The red histogram is preferentially located toward smaller thickness (90th percentile of 2.2 mm for the red versus 90th percentile of 4.5 mm for the blue) suggesting that thinner surviving tissues, whether channels or layers, are more likely to participate in VT pathways. Examining the results of our simulations demonstrated that conduction block was more likely to occur at the exit of thinner tissue layers and channels, where source/sink mismatch is most likely to occur, and hence the subsequent reentries formed after propagation traversed the site of original block. Such behavior is consistent with previous experimental results.³⁵

This study also found that the majority (78%) of the VT pathways were (partially or fully) contained in the subendocardial tissue. Such surviving tissue, likely the result of the diffusion of oxygen from the ventricular

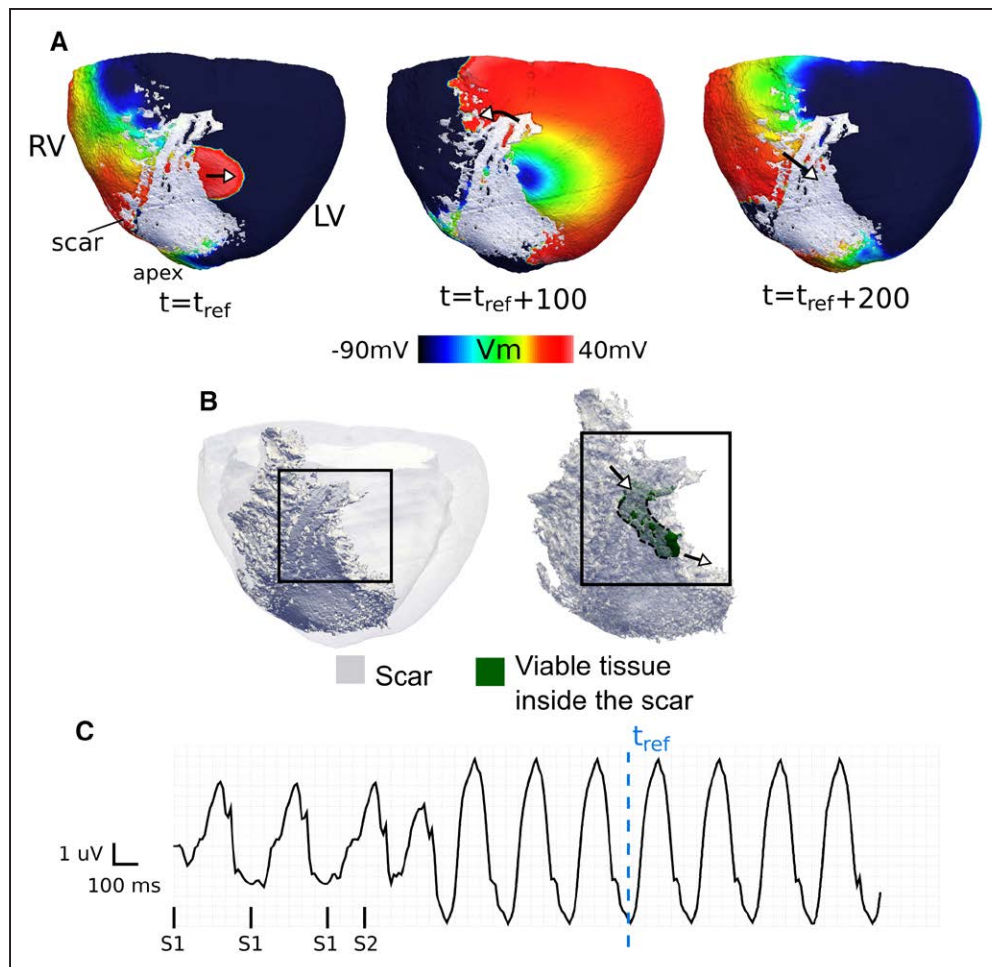


Figure 6. An example of a reentry in heart 7 as viewed from the epicardium (cycle length, 240 ms).

A, Transmembrane voltage maps present snapshots during 1 cycle of reentry with a breakthrough on the epicardium. **B, Left**, View of 3-dimensional model geometry (scar, dark; myocardium, transparent gray); **(right)** delineation of a portion of an intramural surviving tissue embedded inside the infarct (green) that participates in the reentry. The arrows point to the locations of wave entrance and exit from the surviving tissue. **C**, Pseudo-ECG. t_{ref} is the reference time in which the voltage maps in **A** are shown with reference to. LV indicates left ventricle, and RV, right ventricle.

cavity, has been previously found to provide conducting pathways for reentry.^{36,37} Our simulation results showed that the VT pathways could be established primarily contained within the endocardial side of the scar, that is, the layer of subendocardial tissue surrounding the scar. We further demonstrated that the heterogeneous thickness of the subendocardial layer (as revealed by SMLT maps) could create regional heterogeneity in the wave propagation velocity both under pacing activation (Figure III in the [Data Supplement](#)) and during arrhythmia (Figure 4). This provides additional evidence on the importance of the role of local complex infarct structure on the activation properties and propensity for arrhythmia.^{38,39}

Implications for Clinical MRI and VT Substrate Detection

The findings from this study could help bridge the gap between the structure and VT pathways at the submillimeter scale and the corresponding clinical-MRI and

clinical-resolution VT recordings. The SMLT histograms here demonstrate the presence of a significant amount of thin surviving tissue structures surrounding the scar that are otherwise considered subvoxel in a lower resolution clinical LGE-MRI. For example, >70% of the viable tissue surrounding the scar had thickness of <2 mm—such structures would not be directly resolved by imaging with the larger voxel dimensions used in clinical MRI. Importantly, VT pathways were preferentially localized within such structures, suggesting that clinical LGE-MRI techniques need to achieve resolution significantly >2 mm to accurately resolve surviving tissue in the zone of infarct that is part of the VT pathways.

Furthermore, simulations constructed from clinical imaging data are being used to stratify patients with MI for risk of sudden cardiac death³¹ and to potentially guide ablation procedures.⁴⁰ The high-resolution models reconstructed from ex vivo data could help further investigate the effect of image resolution on the VT pathways in patient-specific models. This can be done, for exam-

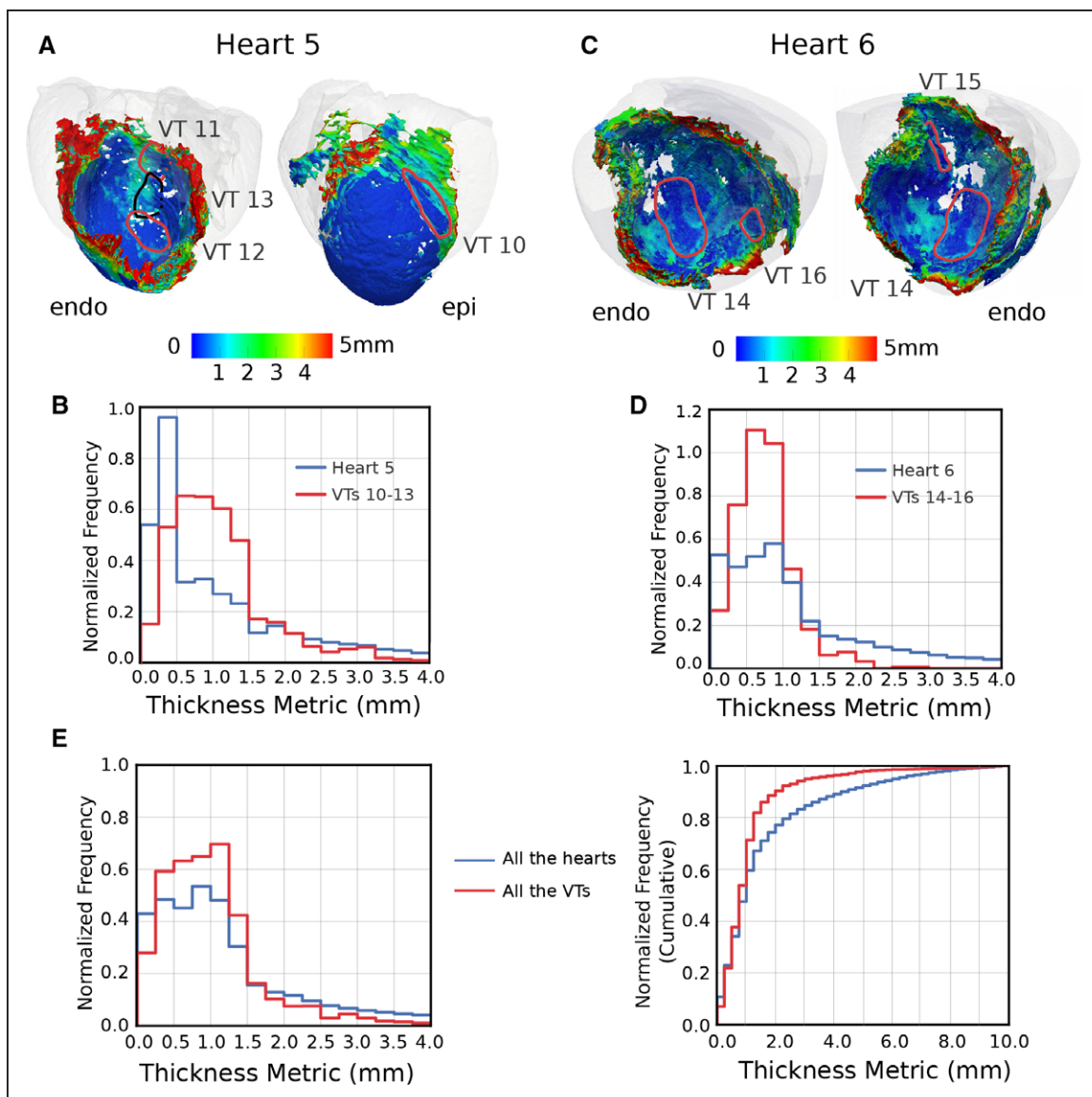


Figure 7. Analysis of the surviving tissue along the ventricular tachycardia (VT) pathways.

A and **C**, Maps of scar-mapped local thickness (SMLT) in 2 hearts with the 3-dimensional (3D) VT pathway loops in each case (myocardium, transparent gray). **B** and **D**, Histograms of frequency of occurrence of a given SMLT value over the entire 3D scar surface (blue) and along the VT pathways (red) in each heart. **E**, The same histograms as **B** and **D** but aggregated for all the hearts and VTs in this study. Shown are normalized (**left**) and cumulative (**right**) histograms.

ple, by retrospective downsampling of the high-resolution images to lower resolution images and simulate and compare VTs in the models constructed at different resolutions.²⁷ Such analysis could, therefore, provide a means to improve the accuracy of the patient-specific models from clinical MRI for the prediction of VT pathways.

Current clinical electrophysiology practice frequently aims to identify channels in the scar, with the notion that terminating propagation through those by ablating tissue will interrupt VT.⁴¹⁻⁴⁵ This study showed that the critical parts of VT reentrant circuit (ie, the VT pathways, as identified here) do not involve all surviving tissue; rather VT pathways are established mostly through surviving tissues of preferential thickness. Thus, as the results obtained here suggest, even if

channels are identified through the scar on the endocardial surface during a clinical electrophysiology procedure, these may be passive conduits of propagation during VT rather than critical pathways and thus not appropriate targets for ablation. Further research will be needed to establish improved strategies for detecting critical VT substrates in cardiac ablation therapy.

Conclusions

In this study, we used a combination of high-resolution (0.25x0.25x0.5 mm³) imaging data and ventricular simulations to systematically and nondestructively characterize the 3D structure of viable tissue in the zone of infarct and explore its role in VT maintenance. Our results from 8

hearts revealed the presence of complex surviving tissue with a thickness of primarily <2 mm in the zone of infarct that provided conducting pathways for VTs. The new knowledge obtained in this study contributes toward a better understanding of infarct-related VTs and could help toward an improved identification of VT substrates.

Study Limitations

The reperfused infarction in porcine—the scans of which were used for model construction—represents the clinical setting in which a coronary occlusion is followed by revascularization; therefore, it may not represent accurately the surviving tissue distribution in the zone of infarct in the human population.

In addition, the spatial resolution of the imaging did not allow for accurately resolving viable tissue structures with dimension of <0.25 mm. Despite that, our results showed that majority of VT pathways were located within surviving tissue of thickness that was >0.25 mm. Indeed, only 7% of the length of the VT pathways was through surviving tissue of thickness ≤0.25 mm. Finally, the Purkinje system is not represented because it cannot be reconstructed from the ex vivo scans—currently, the MRI resolution/contrast does not allow imaging such structures. Future studies are needed to explore the additional role that such system may play in infarct-related VTs.

ARTICLE INFORMATION

Received December 23, 2017; accepted April 5, 2018.

The Data Supplement is available at <http://circep.ahajournals.org/lookup/suppl/doi:10.1161/CIRCEP.117.006131/-DC1>.

Correspondence

Natalia Trayanova, PhD, Department of Biomedical Engineering, Institute for Computational Medicine, Johns Hopkins University, 3400 N Charles St, Baltimore, MD 21218. E-mail ntrayanova@jhu.edu

Affiliations

Department of Biomedical Engineering (F.P., D.A.H., E.R.M., N.A.T.) and Department of Medicine (H.H.), Johns Hopkins University, Baltimore, MD. Departments of Bioengineering, Medicine, and Radiology, University of California, San Diego, La Jolla (E.R.M.).

Acknowledgments

We acknowledge support by the National Institutes of Health Director's Pioneer Award to Dr Trayanova (DP1HL123271) and the support by a grant from the Fondation Leducq.

Disclosures

Dr Trayanova is a cofounder of CardioSolv, LLC, and Dr McVeigh is a cofounder and shareholder of MR Interventions, Inc. CardioSolv and MR Interventions were not involved in this research. The other authors report no conflicts.

REFERENCES

1. John RM, Tedrow UB, Koplan BA, Albert CM, Epstein LM, Sweeney MO, Miller AL, Michaud GF, Stevenson WG. Ventricular arrhythmias and sudden cardiac death. *Lancet*. 2012;380:1520–1529. doi: 10.1016/S0140-6736(12)61413-5.

- Janse MJ, Wit AL. Electrophysiological mechanisms of ventricular arrhythmias resulting from myocardial ischemia and infarction. *Physiol Rev*. 1989;69:1049–1169. doi: 10.1152/physrev.1989.69.4.1049.
- Kléber AG, Rudy Y. Basic mechanisms of cardiac impulse propagation and associated arrhythmias. *Physiol Rev*. 2004;84:431–488. doi: 10.1152/physrev.00025.2003.
- Josephson ME. *Clinical Cardiac Electrophysiology: Techniques and Interpretations*. 4th ed. Philadelphia, PA: Lippincott Williams & Wilkins; 2008:446–642.
- de Bakker JM, van Capelle FJ, Janse MJ, Tasseron S, Vermeulen JT, de Jonge N, Lahpor JR. Slow conduction in the infarcted human heart. 'Zig-zag' course of activation. *Circulation*. 1993;88:915–926.
- Rutherford SL, Trew ML, Sands GB, LeGrice IJ, Smaill BH. High-resolution 3-dimensional reconstruction of the infarct border zone: impact of structural remodeling on electrical activation. *Circ Res*. 2012;111:301–311. doi: 10.1161/CIRCRESAHA.111.260943.
- Connolly AJ, Bishop MJ. Computational representations of myocardial infarct scars and implications for arrhythmogenesis. *Clin Med Insights Cardiol*. 2016;10(suppl 1):27–40. doi: 10.4137/CMC.S39708.
- Ciacco EJ, Ashikaga H, Kaba RA, Cervantes D, Hopenfeld B, Wit AL, Peters NS, McVeigh ER, Garan H, Coromilas J. Model of reentrant ventricular tachycardia based on infarct border zone geometry predicts reentrant circuit features as determined by activation mapping. *Heart Rhythm*. 2007;4:1034–1045. doi: 10.1016/j.hrthm.2007.04.015.
- Smaill BH, Zhao J, Trew ML. Three-dimensional impulse propagation in myocardium: arrhythmogenic mechanisms at the tissue level. *Circ Res*. 2013;112:834–848. doi: 10.1161/CIRCRESAHA.111.300157.
- Connolly A, Trew ML, Smaill BH, Plank G, Bishop MJ. Local gradients in electrotonic loading modulate the local effective refractory period: implications for arrhythmogenesis in the infarct border zone. *IEEE Trans Biomed Eng*. 2015;62:2251–2259. doi: 10.1109/TBME.2015.2421296.
- Kellman P, Arai AE. Cardiac imaging techniques for physicians: late enhancement. *J Magn Reson Imaging*. 2012;36:529–542. doi: 10.1002/jmri.23605.
- Perez-David E, Arenal A, Rubio-Guivernau JL, del Castillo R, Atea L, Arbelo E, Caballero E, Celorrio V, Datino T, Gonzalez-Torrecilla E, Atienza F, Ledesma-Carbayo MJ, Bermejo J, Medina A, Fernández-Avilés F. Noninvasive identification of ventricular tachycardia-related conducting channels using contrast-enhanced magnetic resonance imaging in patients with chronic myocardial infarction: comparison of signal intensity scar mapping and endocardial voltage mapping. *J Am Coll Cardiol*. 2011;57:184–194. doi: 10.1016/j.jacc.2010.07.043.
- Andreu D, Berrueto A, Ortiz-Pérez JT, Silva E, Mont L, Borrás R, de Caralt TM, Perea RJ, Fernández-Armenta J, Zeljko H, Brugada J. Integration of 3D electroanatomic maps and magnetic resonance scar characterization into the navigation system to guide ventricular tachycardia ablation. *Circ Arrhythm Electrophysiol*. 2011;4:674–683. doi: 10.1161/CIRCEP.111.961946.
- Fernández-Armenta J, Berrueto A, Andreu D, Camara O, Silva E, Serra L, Barbarito V, Carotenutto L, Evertz R, Ortiz-Pérez JT, De Caralt TM, Perea RJ, Sitges M, Mont L, Frangi A, Brugada J. Three-dimensional architecture of scar and conducting channels based on high resolution ce-CMR: insights for ventricular tachycardia ablation. *Circ Arrhythm Electrophysiol*. 2013;6:528–537. doi: 10.1161/CIRCEP.113.000264.
- Andreu D, Ortiz-Pérez JT, Fernández-Armenta J, Guiu E, Acosta J, Prat-González S, De Caralt TM, Perea RJ, Garrido C, Mont L, Brugada J, Berrueto A. 3D delayed-enhanced magnetic resonance sequences improve conducting channel delineation prior to ventricular tachycardia ablation. *Europace*. 2015;17:938–945. doi: 10.1093/europace/euu310.
- Estner HL, Zviman MM, Herzka D, Miller F, Castro V, Nazarian S, Ashikaga H, Dori Y, Berger RD, Calkins H, Lardo AC, Halperin HR. The critical isthmus sites of ischemic ventricular tachycardia are in zones of tissue heterogeneity, visualized by magnetic resonance imaging. *Heart Rhythm*. 2011;8:1942–1949. doi: 10.1016/j.hrthm.2011.07.027.
- Piers SR, Tao Q, de Riva Silva M, Siebelink HM, Schalij MJ, van der Geest RJ, Zeppenfeld K. CMR-based identification of critical isthmus sites of ischemic and nonischemic ventricular tachycardia. *JACC Cardiovasc Imaging*. 2014;7:774–784. doi: 10.1016/j.jcmg.2014.03.013.
- Hennig A, Salel M, Sacher F, Camaioni C, Sridi S, Denis A, Montaudon M, Laurent F, Jais P, Cochet H. High-resolution three-dimensional late gadolinium-enhanced cardiac magnetic resonance imaging to identify the underlying substrate of ventricular arrhythmia. *EP Europace*. 2017;gfx303. doi: 10.1093/europace/eux278.

19. Schmidt A, Azevedo CF, Cheng A, Gupta SN, Bluemke DA, Foo TK, Gerstenblith G, Weiss RG, Marbán E, Tomaselli GF, Lima JA, Wu KC. Infarct tissue heterogeneity by magnetic resonance imaging identifies enhanced cardiac arrhythmia susceptibility in patients with left ventricular dysfunction. *Circulation*. 2007;115:2006–2014. doi: 10.1161/CIRCULATIONAHA.106.653568.
20. Roes SD, Borleffs CJ, van der Geest RJ, Westenberg JJ, Marsan NA, Kaandorp TA, Reiber JH, Zeppenfeld K, Lamb HJ, de Roos A, Schalij MJ, Bax JJ. Infarct tissue heterogeneity assessed with contrast-enhanced MRI predicts spontaneous ventricular arrhythmia in patients with ischemic cardiomyopathy and implantable cardioverter-defibrillator. *Circ Cardiovasc Imaging*. 2009;2:183–190. doi: 10.1161/CIRCIMAGING.108.826529.
21. Yan AT, Shayne AJ, Brown KA, Gupta SN, Chan CW, Luu TM, Di Carli MF, Reynolds HG, Stevenson WG, Kwong RY. Characterization of the peri-infarct zone by contrast-enhanced cardiac magnetic resonance imaging is a powerful predictor of post-myocardial infarction mortality. *Circulation*. 2006;114:32–39. doi: 10.1161/CIRCULATIONAHA.106.613414.
22. Pashakhanloo F, Herzka DA, Ashikaga H, Mori S, Gai N, Bluemke DA, Trayanova NA, McVeigh ER. Myofiber architecture of the human atria as revealed by submillimeter diffusion tensor imaging. *Circ Arrhythm Electrophysiol*. 2016;9:e004133. doi: 10.1161/CIRCEP.116.004133.
23. Helm PA, Younes L, Beg MF, Ennis DB, Leclercq C, Faris OP, McVeigh E, Kass D, Miller MI, Winslow RL. Evidence of structural remodeling in the dyssynchronous failing heart. *Circ Res*. 2006;98:125–132. doi: 10.1161/01.RES.0000199396.30688.eb.
24. Pashakhanloo F, Herzka DA, Mori S, Zviman M, Halperin H, Gai N, Bluemke DA, Trayanova NA, McVeigh ER. Submillimeter diffusion tensor imaging and late gadolinium enhancement cardiovascular magnetic resonance of chronic myocardial infarction. *J Cardiovasc Magn Reson*. 2017:1–14.
25. Vadakkumpadan F, Arevalo H, Prassl AJ, Chen J, Kickinger F, Kohl P, Plank G, Trayanova N. Image-based models of cardiac structure in health and disease. *Wiley Interdiscip Rev Syst Biol Med*. 2010;2:489–506. doi: 10.1002/wsbm.76.
26. Arevalo H, Plank G, Helm P, Halperin H, Trayanova N. Tachycardia in post-infarction hearts: insights from 3D image-based ventricular models. *PLoS One*. 2013;8:e68872. doi: 10.1371/journal.pone.0068872.
27. Deng D, Arevalo H, Pashakhanloo F, Prakosa A, Ashikaga H, McVeigh E, Halperin H, Trayanova N. Accuracy of prediction of infarct-related arrhythmic circuits from image-based models reconstructed from low and high resolution MRI. *Front Physiol*. 2015;6:282. doi: 10.3389/fphys.2015.00282.
28. Pop M, Sermesant M, Mansi T, Crystal E, Ghate S, Peyrat JM, Lashevsky I, Qiang B, McVeigh E, Ayache N, Wright GA. Correspondence between simple 3-D MRI-based computer models and in-vivo EP measurements in swine with chronic infarctions. *IEEE Trans Biomed Eng*. 2011;58:3483–3486. doi: 10.1109/TBME.2011.2168395.
29. Plank G, Zhou L, Greenstein JL, Cortassa S, Winslow RL, O'Rourke B, Trayanova NA. From mitochondrial ion channels to arrhythmias in the heart: computational techniques to bridge the spatio-temporal scales. *Philos Trans A Math Phys Eng Sci*. 2008;366:3381–3409. doi: 10.1098/rsta.2008.0112.
30. Vigmond EJ, Aguel F, Trayanova NA. Computational techniques for solving the bidomain equations in three dimensions. *IEEE Trans Biomed Eng*. 2002;49:1260–1269. doi: 10.1109/TBME.2002.804597.
31. Arevalo HJ, Vadakkumpadan F, Guallar E, Jebb A, Malamas P, Wu KC, Trayanova NA. Arrhythmia risk stratification of patients after myocardial infarction using personalized heart models. *Nat Commun*. 2016;7:11437. doi: 10.1038/ncomms11437.
32. Ching-Hsing L, Rudy Y. A dynamic model of the cardiac ventricular action potential simulations of ionic currents and concentration changes. *Circulation*. 1994;74:1071–1098.
33. Ashikaga H, Sasano T, Dong J, Zviman MM, Evers R, Hopenfeld B, Castro V, Helm RH, Dickfeld T, Nazarian S, Donahue JK, Berger RD, Calkins H, Abraham MR, Marbán E, Lardo AC, McVeigh ER, Halperin HR. Magnetic resonance-based anatomical analysis of scar-related ventricular tachycardia: implications for catheter ablation. *Circ Res*. 2007;101:939–947. doi: 10.1161/CIRCRESAHA.107.158980.
34. de Bakker JM, van Capelle FJ, Janse MJ, Wilde AA, Coronel R, Becker AE, Dingemans KP, van Hemel NM, Hauer RN. Reentry as a cause of ventricular tachycardia in patients with chronic ischemic heart disease: electrophysiologic and anatomic correlation. *Circulation*. 1988;77:589–606.
35. Ciaccio EJ, Coromilas J, Wit AL, Peters NS, Garan H. Source-sink mismatch causing functional conduction block in re-entrant ventricular tachycardia. *JACC Clin Electrophysiol*. 2018;4:1–16. doi: 10.1016/j.jacep.2017.08.019.
36. Fenoglio JJ Jr, Pham TD, Harken AH, Horowitz LN, Josephson ME, Wit AL. Recurrent sustained ventricular tachycardia: structure and ultrastructure of subendocardial regions in which tachycardia originates. *Circulation*. 1983;68:518–533.
37. Tschabrunn CM, Roujol S, Nezafat R, Faulkner-Jones B, Buxton AE, Josephson ME, Anter E. A swine model of infarct-related reentrant ventricular tachycardia: electroanatomic, magnetic resonance, and histopathological characterization. *Heart Rhythm*. 2016;13:262–273. doi: 10.1016/j.hrthm.2015.07.030.
38. Ciaccio EJ, Coromilas J, Ashikaga H, Cervantes DO, Wit AL, Peters NS, McVeigh ER, Garan H. Model of unidirectional block formation leading to reentrant ventricular tachycardia in the infarct border zone of postinfarction canine hearts. *Comput Biol Med*. 2015;62:254–263. doi: 10.1016/j.combiomed.2015.04.032.
39. Engelman ZJ, Trew ML, Smail BH. Structural heterogeneity alone is a sufficient substrate for dynamic instability and altered restitution. *Circ Arrhythm Electrophysiol*. 2010;3:195–203. doi: 10.1161/CIRCEP.109.890459.
40. Trayanova NA, Pashakhanloo F, Wu KC, Halperin HR. Imaging-based simulations for predicting sudden death and guiding ventricular tachycardia ablation. *Circ Arrhythm Electrophysiol*. 2017;10:e004743. doi: 10.1161/CIRCEP.117.004743.
41. Calkins H, Epstein A, Packer D, Arria AM, Hummel J, Gilligan DM, Trusso J, Carlson M, Luceri R, Kopelman H, Wilber D, Wharton JM, Stevenson W. Catheter ablation of ventricular tachycardia in patients with structural heart disease using cooled radiofrequency energy: results of a prospective multicenter study. Cooled RF Multi Center Investigators Group. *J Am Coll Cardiol*. 2000;35:1905–1914.
42. Stevenson WG, Friedman PL, Kocovic D, Sager PT, Saxon LA, Pavri B. Radiofrequency catheter ablation of ventricular tachycardia after myocardial infarction. *Circulation*. 1998;98:308–314.
43. Tung R, Josephson ME, Reddy V, Reynolds MR; SMASH-VT Investigators. Influence of clinical and procedural predictors on ventricular tachycardia ablation outcomes: an analysis from the substrate mapping and ablation in Sinus Rhythm to Halt Ventricular Tachycardia Trial (SMASH-VT). *J Cardiovasc Electrophysiol*. 2010;21:799–803. doi: 10.1111/j.1540-8167.2009.01705.x.
44. Andreu D, Penela D, Acosta J, Perea RJ, Soto-iglesias D, Caralt TM De, Ortiz-perez JT, Prat-gonz S, Mont L, Berrueto A. Cardiac magnetic resonance-aided scar dechanneling: influence on acute and long-term outcomes. *Heart Rhythm*. 2017;14:1121–1128. doi: 10.1016/j.hrthm.2017.05.018.
45. Hutchinson MD, Garza HK. Contemporary tools and techniques for substrate ablation of ventricular tachycardia in structural heart disease. *Curr Treat Options Cardiovasc Med*. 2018;20:16. doi: 10.1007/s11936-018-0610-6.

Role of 3-Dimensional Architecture of Scar and Surviving Tissue in Ventricular Tachycardia: Insights From High-Resolution Ex Vivo Porcine Models
Farhad Pashakhanloo, Daniel A. Herzka, Henry Halperin, Elliot R. McVeigh and Natalia A. Trayanova

Circ Arrhythm Electrophysiol. 2018;11:

doi: 10.1161/CIRCEP.117.006131

Circulation: Arrhythmia and Electrophysiology is published by the American Heart Association, 7272 Greenville Avenue, Dallas, TX 75231

Copyright © 2018 American Heart Association, Inc. All rights reserved.

Print ISSN: 1941-3149. Online ISSN: 1941-3084

The online version of this article, along with updated information and services, is located on the World Wide Web at:

<http://circep.ahajournals.org/content/11/6/e006131>

Data Supplement (unedited) at:

<http://circep.ahajournals.org/content/suppl/2018/06/07/CIRCEP.117.006131.DC1>

<http://circep.ahajournals.org/content/suppl/2018/06/07/CIRCEP.117.006131.DC2>

Permissions: Requests for permissions to reproduce figures, tables, or portions of articles originally published in *Circulation: Arrhythmia and Electrophysiology* can be obtained via RightsLink, a service of the Copyright Clearance Center, not the Editorial Office. Once the online version of the published article for which permission is being requested is located, click Request Permissions in the middle column of the Web page under Services. Further information about this process is available in the [Permissions and Rights Question and Answer](#) document.

Reprints: Information about reprints can be found online at:
<http://www.lww.com/reprints>

Subscriptions: Information about subscribing to *Circulation: Arrhythmia and Electrophysiology* is online at:
<http://circep.ahajournals.org/subscriptions/>

Calculation of viable tissue thickness

To characterize the structure of the surviving tissue surrounding the scar, we defined a new *scar-mapped local thickness* (SMLT) metric. This metric was calculated for each node on the 3D scar surface as described below.

First a Euclidean distance map was created by assigning to all the myocardium nodes in the ventricular mesh a value equal to the shortest distance to a boundary surface; here a boundary surface was either the interface of scar and myocardium (scar surface), or the epicardial and endocardial surfaces. Second, at each node on the 3D scar surface, a line was extended within the myocardium in the direction normal to the surface (Figure S2) until it intersected with another boundary surface. The thickness metric was defined to be the minimum of the two values, l and $2d_{max}$, where l is the length of the normal line described above and d_{max} is the maximum of the distance map values calculated at the tissue points traversed by the normal line. In the cases where the local normal to a given surface ends up being nearly perpendicular to the surfaces it intersects, l is an accurate representation of the surviving tissue thickness (Figure S2: l in bottom right). However, in cases where the normal line is oblique to the boundary surface it intersects, it will overestimate the thickness (Figure S2: l' in the bottom left); in this case $2d_{max}$ is selected as the thickness value (as an approximation of the diameter of the largest circle inscribed within the surviving tissue that is tangential to the scar surface node). This method thus provides a metric to quantify the thickness of the surviving tissue surrounding the scar. SMLT values above 10 mm were not included in calculating the aggregated statistics (comprised only 2% of the data).

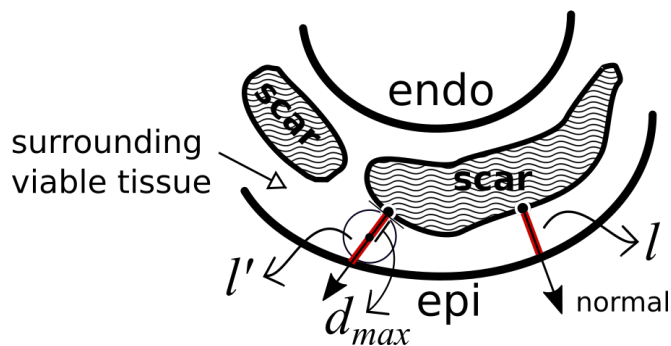


Figure S2. Schematic for SMLT calculation. The process has been illustrated for two representative nodes on the scar (the black arrow lines represent the normal vector to the surface, and the red segments denote the length of the normal between the two boundary surfaces). l and l' are the lengths of the red segments for two cases (see text for detail). The circle on the left shows the largest circle inscribed within the surviving tissue tangential to the scar surface node. d_{max} is the radius of the circle.

Paced propagation in ventricular models

Figure S3 presents paced propagation in two infarcted heart models. Geometries of the 3D heart models are presented in Figure S3-A, showing also the scar color-coded by SMLT values. The activation isochronal maps (Figure S3-B) demonstrate regional activation heterogeneity in the zone of infarct. This heterogeneity is imposed by the complex distribution of the scar and surviving tissue, with isochrone bunching in thin surviving tissue. As demonstrated in heart 5, a thicker region of surviving tissue at the septum (with thickness values of >1 mm) sustains faster propagation relative to those of remote tissue, exacerbating heterogeneity.

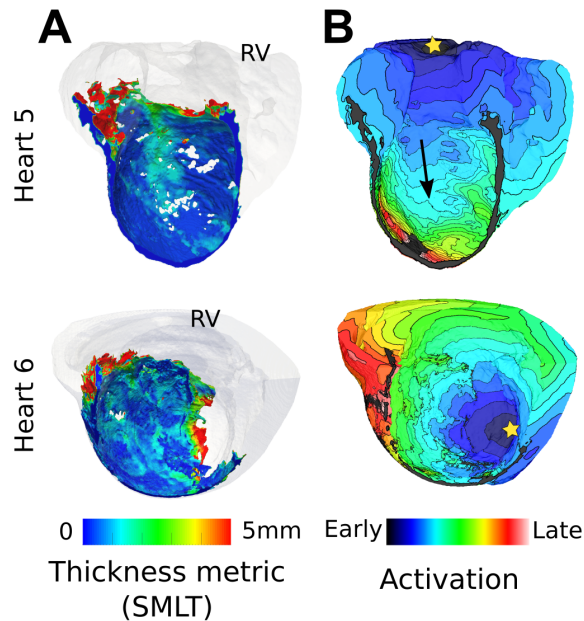


Figure S3. Paced propagation in two infarcted heart models. Results are rendered on a cross-section through the ventricles, with the LV endocardium (septum) exposed. **(A)** 3D ventricular geometry with the scar color-coded with the SMLT metric. Viable tissue is rendered in transparent gray. **(B)** Activation isochrones maps. Stars denote pacing locations. Consecutive contours are 13.3 ms apart.

VT characteristics

Table S1 provides the VT characteristics for the 23 individual VT morphologies in our study. All the VTs in the table were monomorphic and sustained for at least 2 s after the last pacing stimulus. The VTs had an average cycle length (CL) of 190 ± 59 ms, and a mean path length of 53 ± 14 mm. The average conduction velocity on the pathways was 30 ± 8 cm/s. The CL demonstrated a weak to moderate positive correlation with the path length (Pearson correlation = 0.41).

VT #	Heart no.	Pacing Sites	Transmural location (Endo/Trans/Epi)	CL (ms)	Path Length (mm)
1	1	22,24	Epicardial	135	43.7
2	2	11	Endocardial	135	62.5
3	3	10,22,25	Epicardial	135	47.6
4	4	1,6	Endocardial	180	58.7
5	4	2-5,7,10,11,20,21,27	Endocardial	190	43.4
6	4	8,9,14,15,17-19,22-26	Transmural/Epi/Endo	210	68.6
7	4	12	Endocardial	245	43.2
8	4	13	Endocardial	355	49.8
9	4	16	Endocardial	205	35.5
10	5	4	Epicardial	230	73.9
11	5	8	Transmural/Epi/Endo	145	51.5
12	5	12	Endocardial	260	64.9
13	5	21,24	Transmural/Epi/Endo	140	58.4
14	6	5,18,19	Endocardial	295	95.2
15	6	8,13,21,23	Endocardial	165	55.3
16	6	15	Endocardial	145	43.4
17	7	1,5-7,10-13,15-17	Transmural/Epi/Endo	240	58.4
18	7	2-4,8,9,26	Transmural	155	46.7
19	7	25	Transmural/Epi/Endo	160	36.6
20	8	5,6,11,13,16	Epicardial	200	52.6
21	8	7	Endocardial	175	38.2
22	8	20	Epicardial	130	48.5
23	8	23	Endocardial	140	48.6
MEAN \pm SD				190 \pm 59	53 \pm 14

Table S1 Summary of all induced VTs in all models. Pacing sites column presents the locations (see Figure S2 for the definition of site numbers) from which a particular VT morphology was induced. Transmural location column classifies VTs on the basis of wall location relative to the scar (e.g. Endocardial means reentry perpetuated on the endocardial side of the scar). CL: Cycle length.

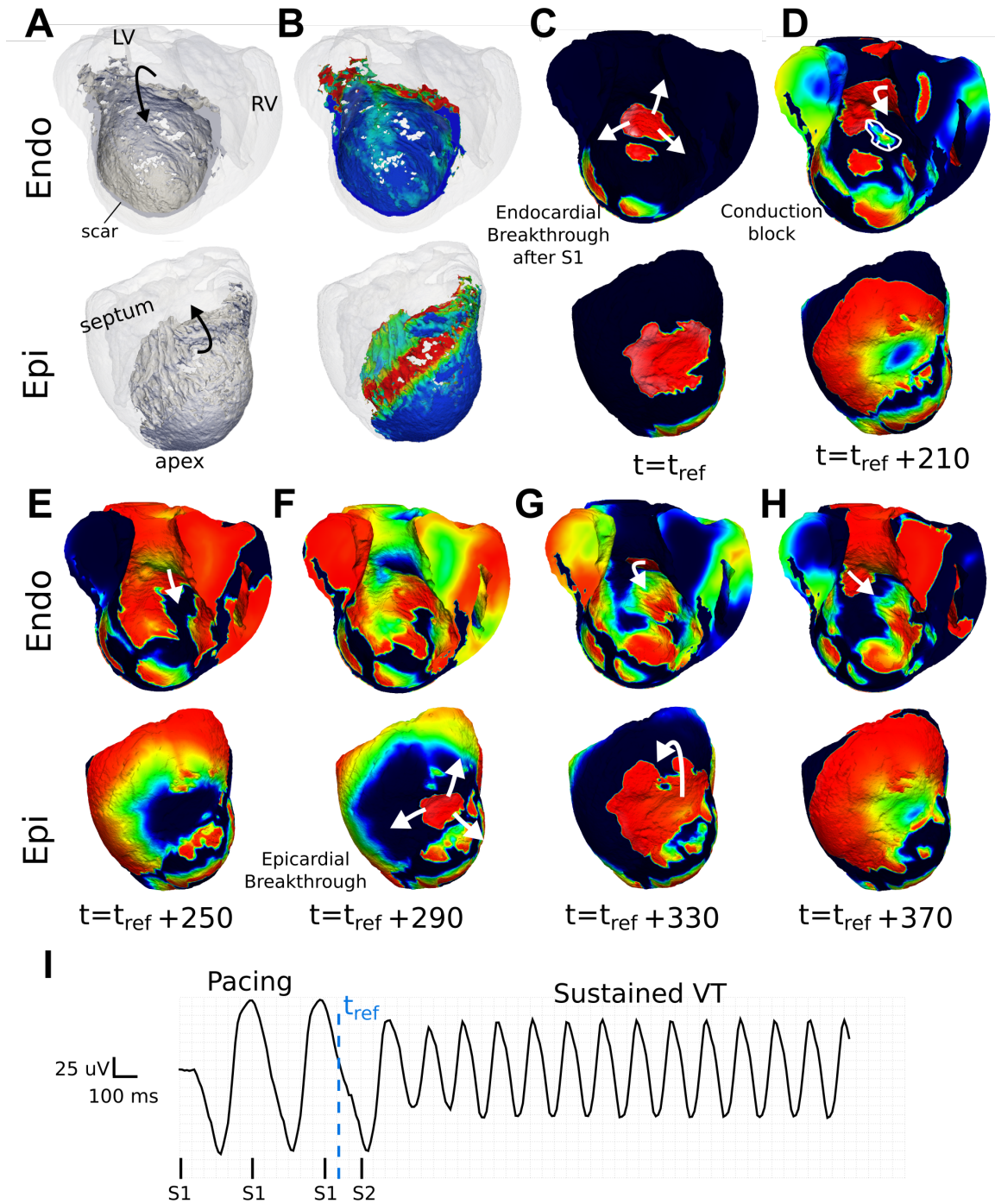


Figure S4 An example of VT (VT #11) with breakthroughs on the epicardial and endocardial surfaces in heart 5 (CL = 145 ms). **(A)** 3D heart geometry **(B)** 3D geometry but with the scar color-coded with the thickness metric **(C)** Endocardial breakthrough following S1 pacing. The breakthrough happens after the wave exits a transmural viable tissue within the infarct. **(D)** Conduction block at the endocardial side of the transmural surviving tissue. **(E-H)** Sustained reentry traversing both the sub-endocardial and the sub-epicardial tissues **(I)** Pseudo-ECG. t_{ref} : reference time.

Supplementary Movies:

Supplementary_MovieS1.mov: VT corresponding to Figure 4 (VT #16).

Supplementary_MovieS2.mov: VT corresponding to Figure 5 (VT #10).

Supplementary_MovieS3.mov: VT corresponding to Figure 6 (VT #17).

References:

1. Pashakhanloo F, Herzka DA, Mori S, Zviman M, Halperin H, Gai N, Bluemke DA, Trayanova NA, Mcveigh ER. Submillimeter diffusion tensor imaging and late gadolinium enhancement cardiovascular magnetic resonance of chronic myocardial infarction. *J Cardiovasc Magn Reson*. 2017;1-14.
2. Heusch G, Skyschally A, Schulz R. The in-situ pig heart with regional ischemia / reperfusion — Ready for translation. *J Mol Cell Cardiol*. 2011;50:951-963.
3. Zhu KQ, J. G, Carrougher R, Gibran NS, Isik FF, Engrav LH. Review of the female Duroc/Yorkshire pig model of human fibroproliferative scarring. *Wound Repair Regen*. 2007;15:S32–S39.
4. Arevalo H, Plank G, Helm P, Halperin H, Trayanova N. Tachycardia in post-infarction hearts: insights from 3D image-based ventricular models. *PLoS One*. 2013;8:e68872.